RSC Advances

PAPER

View Article Online
View Journal | View Issue

Cite this: *RSC Adv.*, 2018, **8**, 3108

Photocatalytic activity of $Ag/Al_2O_3–Gd_2O_3$ photocatalysts prepared by the sol–gel method in the degradation of 4-chlorophenol†

A. Barrera, *[a] F. Tzompantzi,*[b] J. Campa-Molina,[c] J. E. Casillas,[a] R. Pérez-Hernández,[d] S. Ulloa-Godinez,[c] C. Velásquez[e] and J. Arenas-Alatorre[f]

The photocatalytic activity in the degradation of 4-chlorophenol (4-ClPh) in aqueous medium (80 ppm) using 2.0 wt% $Ag/Al_2O_3–Gd_2O_3$ (Ag/Al–Gd-*x*; where x = 2.0, 5.0, 15.0, 25.0 and 50.0 wt% of Gd_2O_3) photocatalysts prepared by the sol–gel method was studied under UV light irradiation. The photocatalysts were characterized by N_2 physisorption, X-ray diffraction, SEM, HRTEM, UV-Vis, XPS, FTIR and fluorescence spectroscopy. About 67.0% of 4-ClPh was photoconverted after 4 h of UV light irradiation using $Ag/\gamma\text{-}-Al_2O_3$. When Ag/Al–Gd-*x* photocatalysts were tested, the 4-ClPh photoconversion was improved and more than 90.0% of 4-ClPh was photoconverted after 3 h of UV light irradiation in the materials containing 15.0 and 25.0 wt% of Gd_2O_3. Ag/Al–Gd-25 was the material with the highest efficacy to mineralize dissolved organic carbon, mineralizing more than 85.0% after 4 h of UV light irradiation. Silver nanoparticles and micro-particles of irregular pentagonal shape intersected by plane nanobelts of $Al_2O_3–Gd_2O_3$ composite oxide were detected in the Ag/Al–Gd-25 photocatalyst. This material is characterized by a lowest recombination rate of electron–hole pairs. The low recombination rate of photo-induced electron–hole pairs in the Ag/Al–Gd-*x* photocatalysts with high Gd_2O_3 contents (≥15.0 wt%) confirmes that the presence of silver nanoparticles and microparticles interacting with $Al_2O_3–Gd_2O_3$ composite oxide entities favors the separation of photo-induced charges (e^- and h^+). These materials could be appropriate to be used as highly efficient photocatalysts to eliminate high concentrations of 4-ClPh in aqueous medium.

Received 22nd November 2017
Accepted 30th December 2017

DOI: 10.1039/c7ra12665d

rsc.li/rsc-advances

Introduction

Nowadays, environmental pollution caused by hazardous substances from wastewater of industrial processes is a worldwide problem. As an example, the emission of phenolic compounds to the wastewater is among the most critical. These contaminant organic compounds are considered to be hazardous wastes, which are highly toxic and difficult to degrade biologically. Among these contaminants, 4-chlorophenol (4-ClPh) is a recalcitrant organic compound and it plays a main role due to its extensive use. The source of these phenolic compound include the wastewater of many industrial processes such as petroleum refining, plastic, resins, textile and pesticide production, paper processing, and carbon liquefaction among others.[1–3] 4-ClPh released to the environment is very stable and persistent for which it has no capability of assimilation requiring a very long time for its natural degradation, therefore it is necessary to find efficient methods for its rapid degradation. It has been attempted to eliminate these recalcitrant organic compounds by physicochemical and biological methods; however, these treatments are not very effective due to their high chemical stability and low biodegradability.[2] Among the new technologies, increased attention has been paid in the last years to the application of photo-catalytic methods as highly efficient advanced oxidation processes (AOP) for eliminating organic pollutants in aqueous wastes.[1–3] The elimination of recalcitrant organic pollutants in aqueous medium is assured since these methods decompose contaminant molecules into harmless compounds. The photo-catalytic method is based on

[a]*Laboratorio de Nanomateriales Catalíticos, Centro Universitario de la Ciénega, Universidad de Guadalajara, Av. Universidad, No. 1115, Col. Linda Vista, C.P. 47820, Ocotlán, Jalisco, México. E-mail: arturo.barrera@cuci.udg.mx; arturobr2003@yahoo.com.mx; Tel: +52 392 92 594 00*

[b]*Depto. de Química, Área de Catálisis, Universidad Autónoma Metropolitana – Iztapalapa, Av. San Rafael Atlixco 189, C.P. 09340, Cd. de México, México. E-mail: fjtz@xanum.uam.mx*

[c]*Laboratorio de Materiales Avanzados, Universidad de Guadalajara Depto. De Electrónica, Blvd. Marcelino García Barragán 1422 esq. Calzada Olímpica, Col. Olímpica 44430, Guadalajara, Jalisco, México*

[d]*Laboratorio de Nanocatálisis, Depto. de Tecnología de Materiales, Instituto Nacional de Investigaciones Nucleares, Carr. México-Toluca S/N, La Marquesa, Ocoyoacac, Edo. De México, C.P. 52750, México*

[e]*Centro de Investigación en Nanociencia y Nanotecnología, Centro Universitario de los Valles, Universidad de Guadalajara, Ameca, Jalisco 46600, México*

[f]*Universidad Nacional Autónoma de México, Instituto de Física, México D.F., México*

† Electronic supplementary information (ESI) available: Additional UV-Vis, XPS, E_g, photolysis, intermediates concentration data. See DOI: 10.1039/c7ra12665d

the use of semiconductor materials as photocatalysts and UV or visible light as irradiation source. Among the photocatalytic materials, TiO_2,[4–6] Bi_2O_4 and Bi_2O_7,[7] and layered double hydroxides[8,9] have been tested for the photodegradation of phenolic compounds in aqueous medium. Alternative, it has been demonstrated in earlier work that in spite that γ-Al_2O_3 is considered as an isolating material, it exhibits high photocatalytic activity in the degradation of contaminant organic molecules in aqueous medium.[10] However, it is necessary to improve the photocatalytic activity of γ-Al_2O_3 because it needs relatively long reaction times to reach a high photoconversion of contaminant organic molecules. One way in order to improve the photocatalytic activity of γ-Al_2O_3 is by addition of rare earth oxides and by coupling the Al_2O_3–Ln_2O_3 composite oxides with noble metal oxides.[11,12] Regarding to it, we have reported in earlier works the use of noble metal oxides such as PdO supported on Al_2O_3–Nd_2O_3 binary oxides prepared by the sol–gel method as interesting co-catalysts for the photodegradation of 2, 4-D and phenol molecules in aqueous medium.[11,12] Concerning to it, it is known that the coupling of semiconductor oxides with noble metals increase their photocatalytic response by reducing the recombination rate of the photogenerated charge carriers.[13–22] In this sense one very attractive noble metal to be used as photocatalytic component is silver due to its remarkable activity and optical properties dependent on its particle size.[23–30] Gadolinium oxide (Gd_2O_3) is another interesting lanthanide oxide which has been used as doping agent of TiO_2 and ZnO semiconductors in order to improve their photocatalytic properties.[31] Gd_2O_3 is attractive due to its high chemical durability although it absorbs UV light in the same region as that of γ-Al_2O_3 and its band gap energy ranges from 3.8 eV to 5.4 eV depending of its structure.[32,33] Although γ-Al_2O_3 is considered as an insulating material it would be very interesting to investigate the influence of Gd_2O_3 addition to γ-Al_2O_3 and the coupling with silver in order to improve the photocatalytic activity of γ-Al_2O_3. In the present work, silver was deposited by impregnation onto Al_2O_3–Gd_2O_3 composite oxides prepared by the sol–gel method to obtain Ag/Al_2O_3–Gd_2O_3 photocatalysts. We assume that the preparation of Al_2O_3–Gd_2O_3 composite oxides by the sol–gel method might result in the obtention of well mixed homogeneous supports with a uniform dispersion of Al_2O_3 and Gd_2O_3 phases and a major interaction with silver species in order to produce the separation of photoinduced (e^-, h^+) charges. The purpose of the present work is the study of the photocatalytic performance of Ag/Al_2O_3–Gd_2O_3 co-catalysts prepared by the sol–gel method in the photodegradation of 4-chlorophenol (4-ClPh) in aqueous medium. The influence of the textural, structural, optical and surface properties of the Ag/Al_2O_3–Gd_2O_3 photocatalysts on their photocatalytic activity in the photodegradation of 4-chlorophenol were studied.

Experimental

Synthesis of Ag/Al–Gd-*x* photocatalysts

Al_2O_3–Gd_2O_3 mixed oxides with different concentration of Gd_2O_3 (Al–Gd-*x*, where x = 2.0, 5.0, 15.0, 25.0, 50.0 wt% of Gd_2O_3) were synthesized by the standard sol–gel method using organic precursors, in brief: a required volume of aluminum tri-*sec*-butoxide, Al(*sec*-but.)$_3$, (Aldrich) was dissolved in a three mouth glass flask containing 10 mL of 2-methylpentane 2,4-diol (JT Baker) as a complexing agent. The precursor solution was heated at 70 °C under continuous stirring for 1 h. After that, the solution was cooled down to 50 °C and then a required amount of gadolinium acetyl-acetonate, Gd(AcAc)$_3$, (Aldrich) previously dissolved in acetone at 40 °C was added. The precursor solution was kept at 50 °C being continuously stirred for 1 h. Then, a volume of 10 mL of deionised water was added to the solution drop wise. The obtained gels were aged at 50 °C for 4 h and then aged again now at 70 °C during 16 h. After that, the solids were dried at 110 °C for 12 h followed by calcination under static air at 650 °C for 4 h to obtain Al_2O_3–Gd_2O_3 composite oxides. Pure Al_2O_3 (Al) was prepared the same method as described above but without the addition of gadolinium acetyl-acetonate. Also, pure Gd_2O_3 (Gd) was prepared by calcination of gadolinium acetyl-acetonate powder at 800 °C by 5 h. Calcined Al_2O_3, Gd_2O_3 and Al–Gd-*x* mixed oxides were impregnated with silver acetyl-acetonate, Ag(AcAc)$_2$ (Aldrich) dissolved in toluene in appropriated amounts to obtain photocatalysts with theoretically 2.0 wt% of Ag_2O. Finally, the impregnated solids were dried at 110 °C for 12 h followed by calcination in an oven at 500 °C for 3 h.

Characterization of Ag/Al–Gd-*x* photocatalysts

Textural properties of Ag/Al and Ag/Al–Gd-*x* photocatalysts were studied by nitrogen physisorption at the saturation temperature of liquid nitrogen (−195.6 °C) by using an Autosorb gas sorption system (IQ model from Quantachrome). Samples were outgassed with He flow at 300 °C for 5 h previous to the measurements. Specific surface area was calculated by using the Brunauer–Emmet–Teller (BET) equation. Pore size distributions were calculated by applying the Barrett, Joyner and Halenda (BJH) method to the desorption branch of nitrogen isotherms.

Structure properties of Ag/Al and Ag/Al–Gd-*x* photocatalysts were studied by X-ray diffraction by using a Theta–Theta model X-ray diffractometer (STOE Gmbh, Germany). X-ray diffraction patterns were recorded at room temperature in the 2θ angle range between 5° and 70°, with a 2θ step of 0.02° and 1s per step point and using a Cu Kα (λ = 0.154 nm) electromagnetic radiation source. Identification of the diffraction peaks from the XRD patterns was carried out using the JCPDS database included in the software of the equipment. Structural properties of Ag/Al and Ag/Al_2O_3–Gd-*x* photocatalysts were also studied by scanning electron microscopy. SEM images of Ag/Al and Ag/Al–Gd-25 photocatalysts were obtained using a scanning electron microscope, HRSEM Jeol 7600F, with a power of 30 kV and a resolution of 1 nm.

TEM images of Ag/Al–Gd-25 sample were also obtained using a TEM JEM2010FEG microscope with a special resolution of 0.19 nm. The sample microstructure of Ag/Al–Gd-25 sample was imaged through high-resolution transmission electron microscopy (TEM) using a Jeol JEM-2010 FEG at 200 or scanning transmission electron microscopy—high angle annular dark

field (STEM-HAADF). For TEM observation, the samples were crushed in ethanol and the solution was ultrasonically stirred before dropping it on a holey carbon-covered copper TEM grid, followed by drying. In order to elucidate the nature of the Ag and Al_2O_3–Gd_2O_3 composite oxide, we perform HAADF analysis (high-angle annular dark-field microscopy) which depends on the atomic numbers of the elements (Z contrast). In the case of Ag/Al_2O_3–Gd_2O_3 catalysts, the difference among the atomic number of the elements makes it possible to observe notable differences in the contrast of the image.

Optical properties of Ag/Al and Ag/Al–Gd-*x* photocatalysts were studied by UV-Vis diffuse reflectance spectroscopy by using an UV-Vis CARY 300 SCAN spectrophotometer in the wavelength range of 190–800 nm with a scan speed of 600 nm min^{-1}; intervals of data collection of 1 nm and a change of the light source at a wavelength of 350 nm.

Surface properties of Ag/Al and Ag/Al–Gd-*x* photocatalysts were studied by XPS. The XPS spectra were recorded on a VG ESCALAB 250 apparatus after excitation with a monochromatic Al Kα radiation ($h\nu = 1486.6$ eV). Samples were embedded onto indium foils which were pressed manually and placed to a holder. Calibration of the energy position of an XPS peak was performed by using the binding energy of carbon 1s peak at 284.8 eV. The unresolved XP spectra for the Gd 3d transition were deconvoluted with two doublets by using a standard Gaussian function. The binding energies values were assigned to the corresponding oxidation state according to literature data. Fluorescence experiments of Al_2O_3, Ag/Al, Ag/Gd and Ag/Al–Gd-*x* photocatalysts were carried out using a Fluorescence Varian Cary eclipse spectrophotometer using an excitation wavelength of 250 nm.

Photocatalytic degradation of 4-chlorophenol

The 4-chlorophenol (4-ClPh) photo-catalytic degradation was carried out using a 1 L batch-type round bottom cylindrical glass photo-reactor surrounded by a double-wall glass jacket. Previous to photo-degradation experiments, an aqueous solution of 4-ClPh (Aldrich) with a concentration of 80 ppm was bubbled with air during 2 h. After that, 200 mL of the 4-ClPh dissolution was put into the glass photo-reactor followed by the addition of 200 mg of either Ag/Al or Ag/Al–Gd photocatalysts to give a concentration of 1 mg of photo-catalyst per mL of 4-ClPh solution. Under continuous aeration (1 mL s^{-1}) and stirring, the 4ClPh dissolution was irradiated using a protected quartz tube with a Pen-Ray UV power supply lamp (UVP products) of a typical wavelength of 254 nm and an intensity of 4400 $\mu W\ cm^{-2}$, immersed into the solution. Prior to the photo-catalytic experiments, the 4-ClPh solution and the photocatalyst were kept in contact for 1 h without irradiation in order to determine the adsorption capacity of the solids. Then, the UV lamp was turned on. To follow the photo-degradation of 4-ClPh as a function of time, samples of the irradiated solution were taken each hour from the photo-reactor using a filter for a period of 5 h. The 4-ClPh degradation was followed by UV-Vis spectroscopy, employing a CARY 100 spectrophotometer measuring the absorbance at $\lambda = 279$ nm and using the Lambert and Beer equation for the calculation of the concentration of photo-converted 4-ClPh. The relative concentration (C/C_0) data of photo-converted 4-ClPh were adjusted to a first order kinetics of Langmuir–Hinshelwood model type. The total organic carbon (TOC) was followed using a TOC-V_{CEN} Shimadzu 5000 analyzer (catalytic oxidation on Pt at 680 °C). Calibration runs were performed injecting known amounts of potassium phthalate.

Results and discussion

Textural properties of Ag/Al–Gd-*x* photocatalysts

Fig. 1A shows the N_2 adsorption–desorption isotherms of Ag/Al and Ag/Al–Gd-*x* photocatalysts. The isotherms are of the type IV corresponding to mesoporous materials according to the IUPAC classification.[34] The hysteresis loop is changing from the H1-type at low Gd_2O_3 concentration to the H2-type at high Gd_2O_3 concentration in the Ag/Al–Gd-*x* materials.[35] The maximum of the modal peak of the pore size distributions of Ag/Al–Gd-*x* photocatalysts is shifted to a less pore size with the increase in the Gd_2O_3 concentration (Fig. 1B).

The S_{BET} of Ag/Al (261.0 $m^2\ g^{-1}$) is improved with addition of a low concentration of Gd_2O_3 to obtain a maximum (S_{BET} = 270.0 $m^2\ g^{-1}$) in the Ag/Al–Gd-5 photocatalyst (Table 1). At higher concentration of Gd_2O_3, the S_{BET} of the materials decreased to a minimum S_{BET} as observed in the bare Ag/Gd_2O_3 ($S_{BET} = 2.0$). Such improvement in the S_{BET} at low concentration of Gd_2O_3 in the Ag/Al–Gd-*x* photocatalysts indicates that Gd_2O_3 acts as a textural promoter of γ-Al_2O_3.

The total specific pore volume of Ag/Al ($V_{PT} = 0.85\ m^2\ g^{-1}$) is also improved with addition of a low concentration of Gd_2O_3 with the maximum ($V_{PT} = 1.24\ cm^3\ g^{-1}$) observed in Ag/Al–Gd-2. At higher Gd_2O_3 concentrations the V_{PT} decreased to a minimum value ($V_{PT} = 0.001\ cm^3\ g^{-1}$) observed in the bare Ag/Gd_2O_3.

The average pore diameter of Ag/Al (APD = 13.0 nm) is also increased with addition of a low concentration of Gd_2O_3 obtaining a largest APD in Ag/Al–Gd-2 (APD = 18.2 nm) corroborating the highest V_{PT} observed for this material

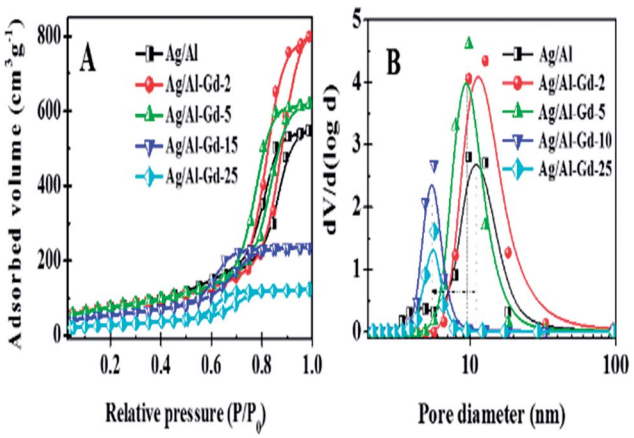

Fig. 1 (A) Nitrogen adsorption–desorption isotherms of Ag/Al–Gd-*x* photocatalysts; (B) pore size distributions of Ag/Al–Gd-*x* photocatalysts.

Table 1 Textural properties of Ag/Al–Gd-*x* photocatalysts prepared by the sol–gel method

Co-catalyst	S_{BET} ($m^2\ g^{-1}$)	V_{PT} ($cm^3\ g^{-1}$)	APD (nm)
Ag/Al_2O_3	261.0	0.85	13.0
Ag/Al–Gd-2	268.7	1.24	18.4
Ag/Al–Gd-5	270.4	0.96	14.1
Ag/Al–Gd-15	192.0	0.37	7.7
Ag/Al–Gd-25	101.0	0.19	7.6
Ag/Al–Gd-50	112.0	0.23	8.2
Ag/Gd_2O_3	0.6	0.004	25.0

(Table 1). At higher Gd_2O_3 content the APD decreased to 7.6–8.2 nm observed in silver photocatalysts containing 15.0–50.0 wt% of Gd_2O_3.

The tendency in the decrease of average pore diameter for high Gd_2O_3 concentration corroborates the shift in the decrease in the maximum of the modal peak of pore size distributions.

Structural properties of Ag/Al–Gd-*x* photocatalysts

XRD patterns of Ag/Al–Gd-*x* photocatalysts prepared by the sol–gel method are shown in Fig. 2. XRD pattern of pure Ag/Al shows diffraction peaks at 2θ = 33.1, 37.6, 46.3, and 66.7° corresponding to crystalline planes of γ-Al_2O_3 phase (JCPDS card: 10-0425). Whereas the XRD pattern of pure Ag/Gd shows diffraction peaks corresponding to crystalline planes of Gd_2O_3 with a cubic structure (JCPDS 12-0797). The diffraction peaks of γ-Al_2O_3 are also observed in the XRD patterns of Ag/Al–Gd-*x* photocatalysts, however, their intensities decrease with the increase in the Gd_2O_3 concentration. When the concentration of Gd_2O_3 is higher than 15.0 wt%, the diffraction peaks of γ-Al_2O_3 are almost planes and the XRD patterns being nearly similar to those shown by the disordered materials showing a lack of structural periodicity of long-range order. Not any diffraction peak corresponding to Gd_2O_3 phase is observed in the XRD patterns of Ag/Al–Gd-*x* photo-catalysts suggesting that amorphous Gd_2O_3 particles are homogeneously well mixed with the γ-Al_2O_3 agglomerates.

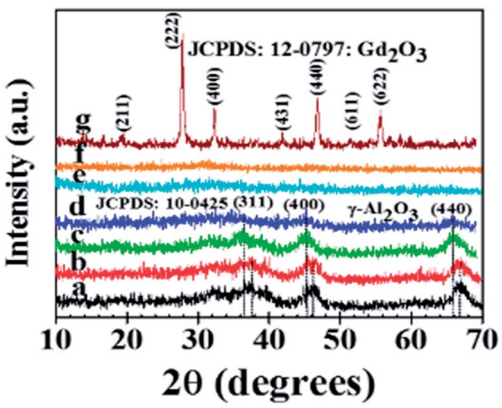

Fig. 2 X-ray diffraction patterns of the Ag/Al–Gd-*x* photocatalysts: (a) Ag/Al_2O_3; (b) Ag/Al–Gd-2; (c) Ag/Al–Gd-5; (d) Ag/Al–Gd-15; (e) Ag/Al–Gd-25; (f) Ag/Al–Gd-50; (g) Ag/Gd_2O_3.

Moreover, it is observed a slight shifting in the diffraction peaks of γ-Al_2O_3 to lower 2θ angles in the XRD patterns of Ag/Al–Gd-*x* photocatalysts with 5.0 and 15.0 wt% of Gd_2O_3 indicating the incorporation of silver in the Al–Gd-*x* composite lattice. On the other hand, not any diffraction peak corresponding to silver phases were observed in the XRD patterns of either Ag/Al or Ag/Al–Gd-*x* photocatalysts which could be due to either the low concentration of silver (2.0 wt%), which is below of the limit of detection of the equipment, or to that small silver nanoparticles are present in the materials. This is confirmed by Z-contrast STEM image obtained by HAADF of Ag/Al–Gd-25 sample (Fig. 3A) showing a high dispersion of silver nanoparticles with sizes between 2.0 and 7.0 nm that are deposited on strongly scattering Al_2O_3–Gd_2O_3 composite oxide. Whereas, HRTEM micrograph of Ag/Al–Gd-25 sample shows that silver nanoparticles of spherical and irregular pentagonal shapes of approximately 6.0 nm in size are formed which are deposited on the surface of the amorphous Al_2O_3–Gd_2O_3 composite oxide (Fig. 3B). The magnification of the region of one nanoparticle depicted by the square in Fig. 3B shows the presence of rows of diffraction points, which are characteristic of the crystalline lattice planes. The measurement of the lattice distances in the region limited by the square indicates that they have *d*-spacings of 0.2016 and 0.2170 nm. These interplanar distances correspond to the *hkl*(200) and *hkl*(111) planes of the FCC structure of silver nanoparticles (JCPDS card: 04-0783). Furthermore, SEM micrograph of Ag/Al sample (Fig. 4) shows that silver microparticles are also deposited on the surface of amorphous γ-Al_2O_3 agglomerates as observed by the bright white spots of approximately 1.0–3.0 μm in size. A linear scanning by element through the bright white spots indicates that they are composed mostly by metallic silver since the maximum of the linear scanning at about 15.0 μm denoted in color red (Fig. 4a) corresponding to silver coincides with the minimum of the linear scanning at about 15.0 μm in color green corresponding to oxygen (Fig. 4b). Therefore, it is inferred that metallic silver micro-particles are also present on the surface of pure Ag/Al_2O_3. This assumption is also inferred because the maximum of the linear scanning at about 4.0, 12.0 and 18.0 μm in color green belonging to oxygen (Fig. 4b) coincides with the maximum of the linear scanning at the same position in color blue corresponding to aluminum of γ-Al_2O_3 (Fig. 4c).

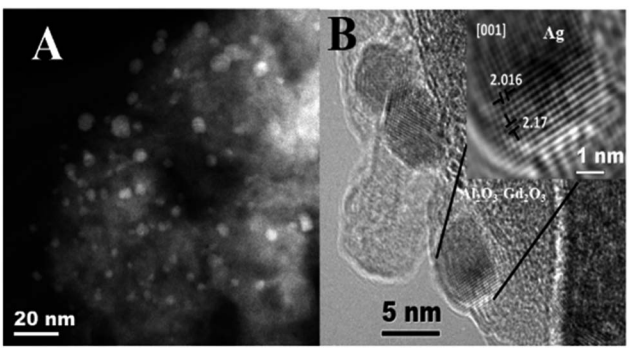

Fig. 3 (A) HAADF STEM image of Ag/Al–Gd-25 photocatalyst; (B) HRTEM image of Ag/Al–Gd-25 photocatalyst.

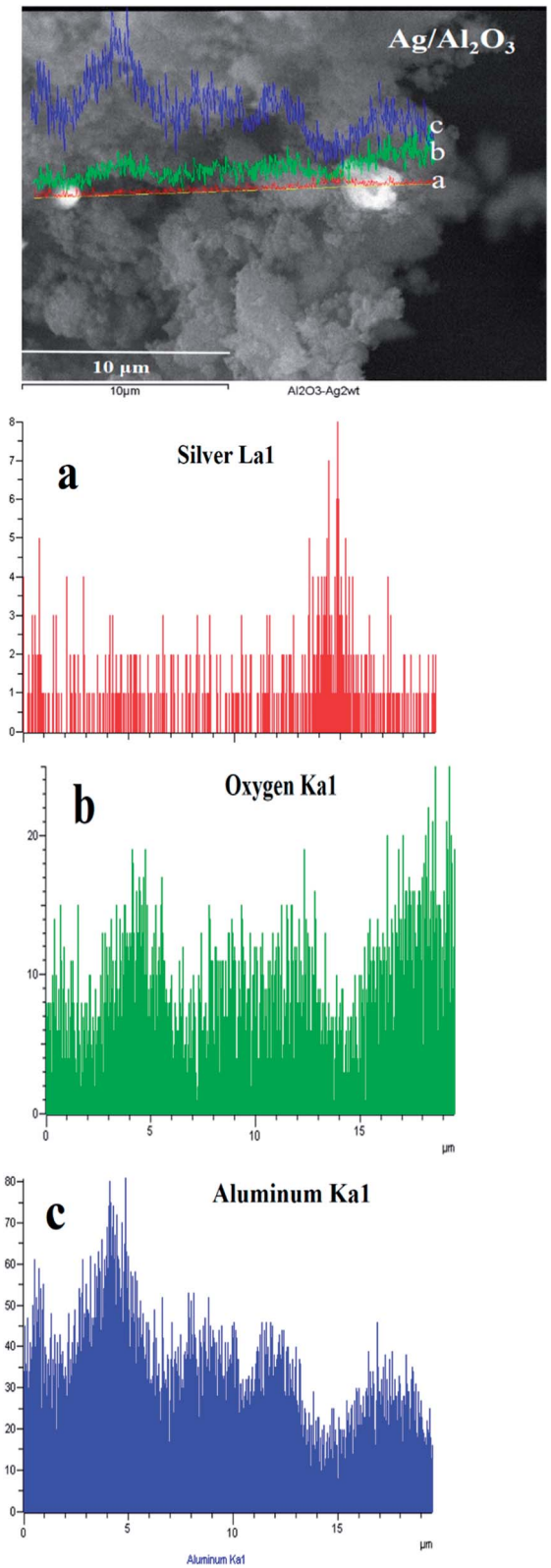

Fig. 4 SEM micrograph of the Ag/Al photocatalyst with linear scanning by element: (a) silver La1; (b) oxygen Ka1; (c) aluminum Ka1.

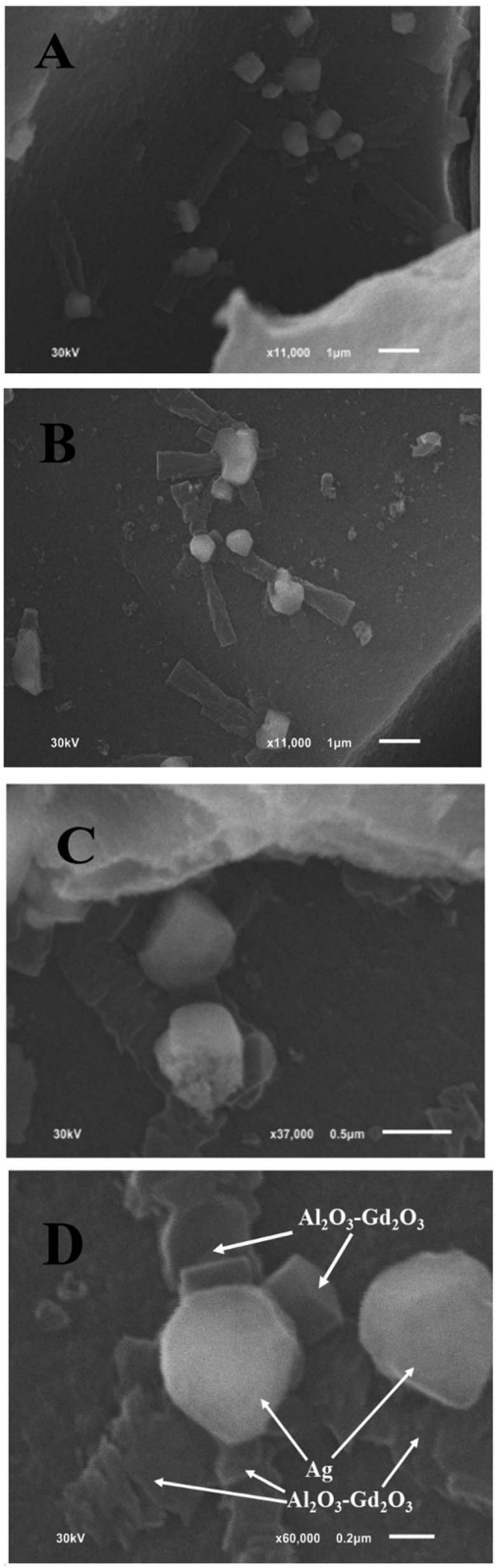

Fig. 5 SEM micrographs of Ag/Al–Gd-25 photocatalyst: (A) ×11 000; (B) ×11 000; (C) ×37 000; (D) ×60 000.

On the other hand, SEM micrographs of Ag/Al–Gd-25 sample (Fig. 5A and B) show a high dispersion of silver particles. Furthermore, these SEM micrographs show that plane nano-belts of approximately 2.5 μm in length are formed which are oriented and intersected with silver micro-particles of approximately 0.6 μm in size. Moreover, the magnification of one of the

regions in the SEM micrograph of Fig. 5A and B shows that some amorphous particles and some quasi-crystalline micro-particles of irregular pentagonal shape are formed which are intersected by the plane nano-belts (Fig. 5C and D). It seems that the plane nano-belts are formed by stacking of tiny material blocks that are self-assembled and oriented to the particles of pentagonal shape, some of which are found still in an amorphous state just in the process of formation. Therefore, it can be inferred that the pentagonal particles might be the seed of nucleation for the self-assembled plane nano-belts or that the stacking and orientation of plane nano-belts intersecting the micro-particles would produce their pentagonal shapes. The EDS elemental composition from the region shown in the SEM micrograph of Fig. 5D indicates that the bright pentagonal particles are composed mostly by a rich content of silver (16.42 wt%). Whereas, the plane nano-belts formed by stacking of material are composed mainly by 72.9 wt% of Al_2O_3 and 21.7 wt% of Gd_2O_3.

Optical properties of Ag/Al–Gd-*x* photocatalysts

Fig. S1† shows the UV-Vis spectra of γ-Al_2O_3 and Al–Gd-*x* composite oxides, whereas inset the UV-Vis spectra of bare Gd_2O_3. UV-Vis spectrum of γ-Al_2O_3 shows a broad absorption band at about 264.0 nm with an absorption edge located at wavelengths between 290.0 and 350.0 nm that is attributed to charge transfer or the presence of a high density of defects in the structure of γ-Al_2O_3.[36] Whereas, the UV-Vis spectrum of Gd_2O_3 exhibits an intense and broad absorption band at about 232.0 nm and two small sharp peaks located at 277.0 nm and 313.0 nm. The sharp peak at about 277 nm is assigned to the $^8S_{7/2}$ to ^6I_J Gd^{3+} transition of Gd_2O_3.[37] Similar to γ-Al_2O_3, UV-Vis spectra of Al–Gd composite oxides also show a broad absorption band in the UV region with an absorption edge located between 290.0 and 350.0 nm whose intensity increases due to the overlap with the absorption bands of Gd_2O_3. UV-Vis spectra of Ag/Al, Ag/Al–Gd-*x* and Ag/Gd photocatalysts are shown in Fig. 6. These spectra also show absorption bands in the same UV region as γ-Al_2O_3 and Al–Gd-*x* composite oxides, however the absorption bands are located at about 219.0 and 255.0 nm due to the presence of silver species (Fig. 6). The high energy absorption band located at about 219.0 nm is assigned to the electronic transition from $4d^{10}$ to $4d^9$ $5s^1$ orbital of Ag^0 nanoparticles.[38,39] Whereas, the absorption band at about 255.0 nm is attributed to the presence of $Ag_n^{\delta+}$ clusters.[40] The absorption edge located between 255.0 and 310.0 nm in the UV-Vis spectra of Ag/Al is shifted to higher wavelengths in the Ag/Al–Gd-*x* photocatalysts. Furthermore, Ag/Al–Gd-25 sample exhibits some low intensity absorption bands located in the visible region at about 387.0, 483.0, 540.0, and 720.0 nm. These low energy absorption features are attributed to the surface plasmon resonance absorption of surface metallic silver particles.[41] It is clear from UV-Vis spectra of Ag/Al–Gd-*x* photocatalysts that $Ag_n^{\delta+}$ clusters, metallic silver nanoparticles and micro-particles are present on the surface of Ag/Al–Gd-*x* photocatalysts.

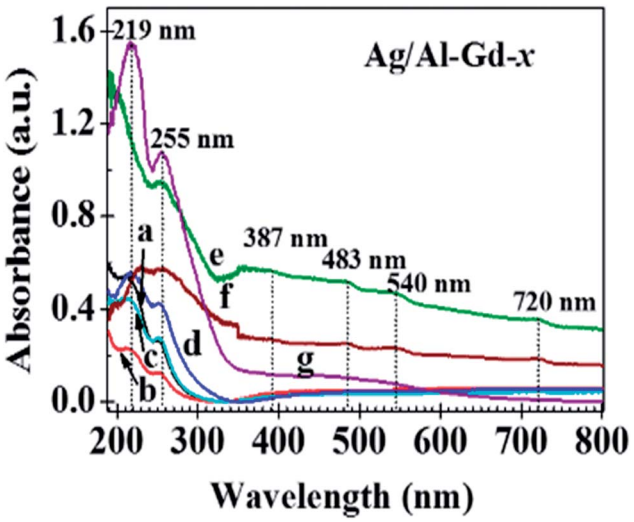

Fig. 6 UV-Vis spectra of Ag/Al–Gd-*x* photocatalysts: (a) Ag/Al; (b) Ag/Al–Gd-2; (c) Ag/Al–Gd-5; (d) Ag/Al–Gd-15; (e) Ag/Al–Gd-25; (f) Ag/Al–Gd-50; (g) Ag/Gd.

Chemical state of surface silver, gadolinium and aluminum species

XPS experiments were carried out in order to get an insight of the chemical state of silver particles on the surface of Ag/Al–Gd-*x* photocatalysts. Fig. 7A shows the high resolution XPS spectrum of the Ag 3d transition of Ag/Al–Gd-25 photocatalyst. The XPS spectrum exhibits two peaks at about 368.48 eV and 374.48 eV with an energy gap between maximums of 6.0 eV. This gap is characteristic of oxidation states of silver and corresponds to the energy spin–orbit splitting generating the Ag $3d_{5/2}$

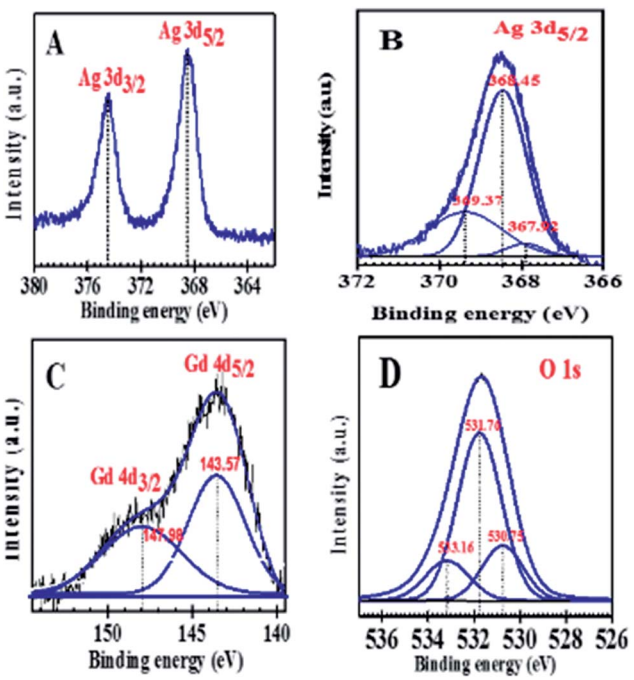

Fig. 7 XPS spectra of Ag/Al–Gd-25 photocatalyst: (A) Ag 3d; (B) Ag $3d_{5/2}$; (C) Gd 4d; (D) O 1s.

and Ag $3d_{3/2}$ transitions.[42] The Ag $3d_{5/2}$ transition is the most usually used to determine the oxidation state of silver. Therefore, this transition was used in order to know the oxidation state of silver species deposited on the surface of the Ag/Al–Gd-25 photocatalyst. The deconvolution of the XPS Ag $3d_{5/2}$ spectrum by a standard gauss function resulted in two doublets (Fig. 7B). The binding energy of the main component of the Ag $3d_{5/2}$ transition is located at about 368.45 eV and it is assigned to pure metallic silver.[43] Whereas the smaller peak located at 367.92 eV has negative shift with respect to the binding energy of the main component and it is assigned to Ag^+ ions.[44] However, the intensity of the peak at 367.92 eV is too small, therefore the presence of Ag^+ ions is nearly negligible on the surface of the material. A third XPS fitted peak located at 369.37 eV is attributed to charge transfer states of metallic silver.[43] Therefore, the study of the chemical state of surface silver species over the Ag/Al–Gd-25 photocatalyst indicates that silver is found predominately in a metallic state. This is also corroborated in the XPS Ag 3d spectrum of bare Ag/Al (Fig. S2†) showing two peaks located at 368.3 and 374.3 eV with a energy gap between them of 6.0 eV that is typical of Ag $3d_{5/2}$ and Ag $3d_{3/2}$ transitions of Ag^0.[42] High resolution XPS spectrum of Gd 4d region (Fig. 7C) was performed in order to determine the chemical state of Gd species on the surface of Ag/Al–Gd-25 photocatalyst. The peaks at 147.98 and 143.57 eV corresponds to Gd $4d_{3/2}$ and Gd $4d_{5/2}$ transitions of Gd_2O_3 respectively.[45–49]

This corroborates that Gd_2O_3 species are present on the surface of Ag/Al–Gd-25 photocatalyst and make up the Al_2O_3–Gd_2O_3 nanobelts. The presence of Gd_2O_3 is also corroborated from the O 1s spectrum (Fig. 7D). This spectrum shows three peaks, one peak situated at 530.75 eV corresponds to the oxygen in Gd_2O_3.[49] The main peak at 531.76 eV is assigned to atomic oxygen in the γ-Al_2O_3 lattice.[50] Whereas the peak located at 533.16 eV is attributed to adsorbed molecular H_2O.[51]

On the other hand, the effect of Ag and Gd_2O_3 on the elemental states of Al in Al_2O_3 is shown in Fig. 8A and B. Fig. 8A shows the XPS Al 2p spectrum of Ag/Al photocatalyst which is fitted in two peaks located at 75.0 eV and 75.6 eV. These binding energies corresponds to γ-Al_2O_3 and $Al(OH)_3$ respectively.[52,53] Whereas, the fitted XPS Al 2p spectrum of Ag/Al–Gd-25 material (Fig. 8B) shows three peaks located at 74.6, 76.2 and 77.5 eV that are assigned to γ-Al_2O_3, $Al(OH)_3$ and anhydride Al_2O_3 respectively.[54,55] As it can be seen, Ag and Gd_2O_3 influence the elemental chemical state of Al, when Gd_2O_3 is added to Al_2O_3, the binding energies of Al in the fitted XPS spectrum of Ag/Al–Gd-25 material change, the peak of γ-Al_2O_3 change to less binding energy (E_b = 74.6 eV) compared to that of Ag impregnated onto bare γ-Al_2O_3 (E_b = 75.0 eV). Whereas, the peak of $Al(OH)_3$ located at 75.6 eV in the fitted XPS spectra of Ag/Al_2O_3 changes to a higher binding energy (E_b = 76.2 eV) in the Ag/Al–Gd-25 material. In addition other fitted XPS peak appear at 77.5 eV in the XPS spectrum of Ag/Al–Gd-25 which is attributed to anhydride Al_2O_3.

The presence of anhydride Al_2O_3 suggests the loss of hydroxyl groups of Al_2O_3 due to the addition of Gd_2O_3 to form the Al_2O_3–Gd_2O_3 composites.

This is corroborated from the FTIR experiments of Ag/Al–Gd-*x* photocatalysts (Fig. 9), the intense band located at about 3500 cm^{-1} in the FTIR spectrum of Ag/Al (Fig. 9a) that is assigned to the stretching vibration mode of OH groups became weaker with increasing the concentration of Gd_2O_3 in the Ag/Al–Gd-*x* photocatalysts and nearly disappeared in Ag/Al–Gd-25 photocatalyst (Fig. 9d) inferring that the coupling between Gd_2O_3 and γ-Al_2O_3 caused the dehydroxylation of the γ-Al_2O_3 surface. The same occurred with the FTIR band located at about 1694 cm^{-1} which corresponds to the bending vibration of OH groups. The loss of OH groups on the surface of Ag/Al–Gd-*x* photocatalysts for high Gd_2O_3 contents (>15.0 wt%) indicates that Gd_2O_3 caused the elimination of hydroxyl groups of alumina. On the other hand, the band at 1528 cm^{-1} is due to CO_3^{2-} vibrations.[33] CO_3^{2-} groups could be arisen from residual carbon of the solvent used in the synthesis of the materials, however they are also eliminated at high Gd_2O_3 concentration.

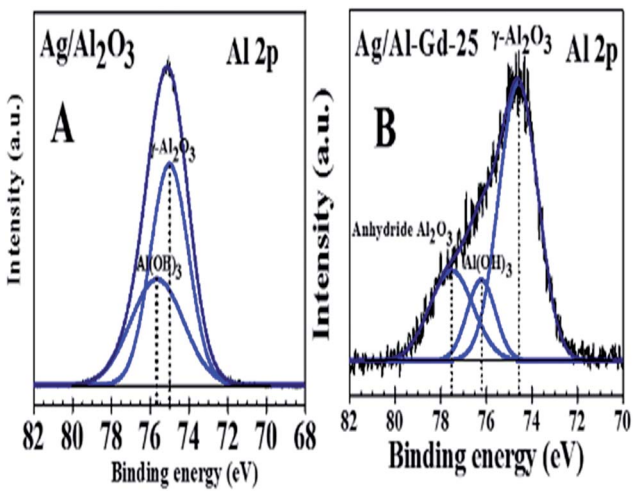

Fig. 8 XPS spectra of Al 2p for: (A) Ag/Al_2O_3; (B) Ag/Al–Gd-25.

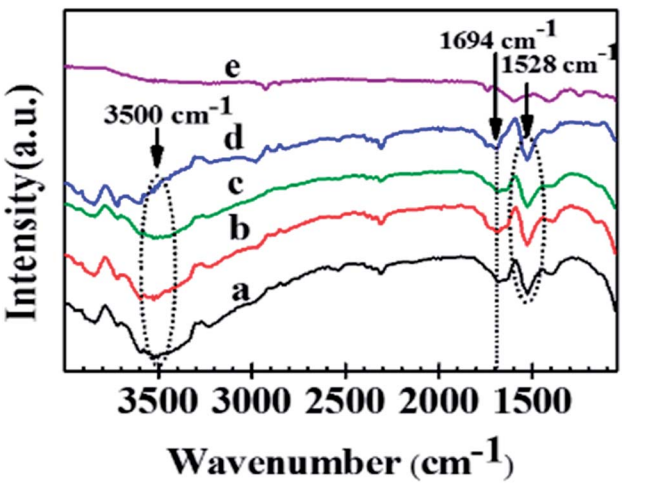

Fig. 9 FTIR spectra of Ag/Al–Gd-*x* photocatalysts: (a) Ag/Al; (b) Ag/Al–Gd-2; (c) Ag/Al–Gd-5; (d) Ag/Al–Gd-15; (e) Ag/Al–Gd-25.

Photocatalytic activity test in the degradation of 4-chlorophenol

Previous studies concerning to the photo-catalytic activity of Ag/Al–Gd-*x* photocatalysts in the degradation of 4-ClPh, it was shown that 4-ClPh molecules in aqueous medium (80 ppm) were not photo-degraded by UV electromagnetic radiation alone without the presence of any photocatalyst (Fig. S3†). It was observed that a modification of the organic molecule occurred with the UV light irradiation, however, the UV light irradiation was not capable to photodegradate such organic molecule. In order to know the adsorption capability of Ag/Al–Gd-*x* photocatalysts, the aqueous 4-ClPh solutions where submitted to a continuous stirring alone without any UV light irradiation (dark light) during 1 h before starting the photo-degradation experiments. The 4-ClPh adsorption capability of γ-Al_2O_3 was about 27.0% (Table 2). However, the adsorption capability over Ag/Al decreased to 20.0% (Fig. 10, 11; Table 3). Furthermore, when Ag/Al–Gd-*x* photocatalysts were used, the adsorption capability of 4-ClPh greatly decreased to less than 6.0% indicating that the adsorption phenomena on the surface of Ag/Al–Gd-*x* photocatalysts was inhibited significantly by coupling Gd_2O_3 to γ-Al_2O_3 by the sol–gel method. Each one of adsorption percentage values of 4-ClPh shown by the photocatalysts was substracted from their corresponding photoconversion percentages during photodegradation in order to obtain the real photoconversion of 4-ClPh over the photocatalysts (Table 2). As shown in the UV-Vis spectrum of photoirradiated 4-ClPh over Ag/γ-Al_2O_3 (Fig. 10A), the intensity of the absorption band at about $\lambda = 279$ nm decreased uniformly with irradiation time showing the decomposition of 4-ClPh molecules. The relative concentration of 4-ClPh decreased uniformly with irradiation time in the Ag/Al photocatalyst to reach a C/C_0 equal to 0.33 after 4 h of UV light irradiation (Fig. 11). However, when the Ag_2O/Al–Gd-*x* photocatalysts were used, the intensity of the absorption band at about 279 nm in the UV-Vis spectra of photoirradiated 4-ClPh over Ag/Al–Gd-25 photocatalyst decreased more deeply and almost disappeared after just 3 h of reaction (Fig. 10B). The relative concentration was about 0.1 at 3 h of UV light irradiation in the Ag/Al–Gd-*x* photocatalysts with

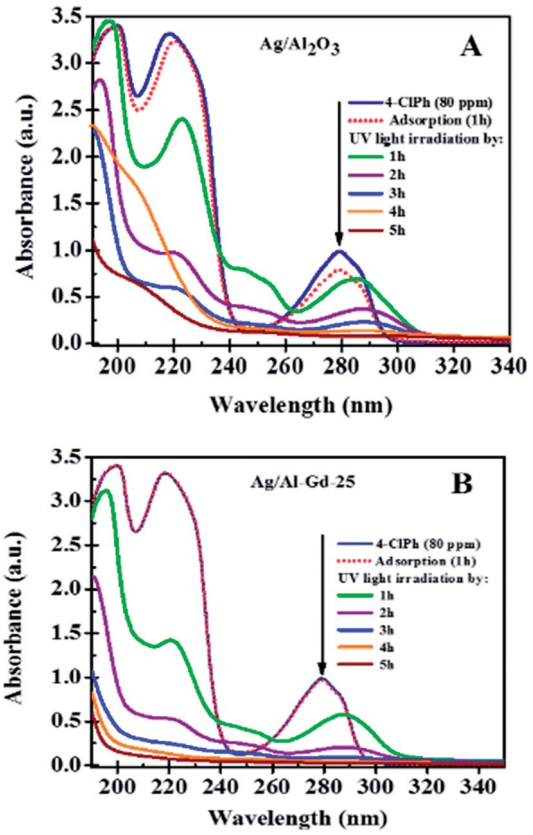

Fig. 10 UV-Vis spectra of 4-chlorophenol after UV light irradiation by 5 h using: (A) Ag/Al_2O_3 and (B) Ag/Al–Gd-25 photocatalysts.

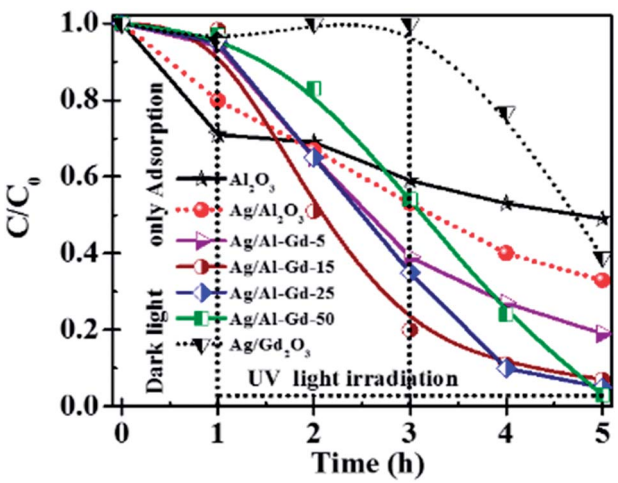

Fig. 11 Relative concentration of 4-chlorophenol as a function of dark light and UV light irradiation time over Ag/Al–Gd-*x* photocatalysts prepared by the sol–gel method.

Table 2 Adsorption% and 4-chlorophenol% over Ag/Al–Gd-*x* photocatalysts prepared by the sol–gel method

Co-catalyst	Adsorption% dark light during 1 h	4-Chlorophenol photoconversion% with UV light irradiation during: 1 h	2 h	3 h	4 h
Al_2O_3	29.0	31.0	41.0	47.0	51.0
Ag/Al_2O_3	20.0	33.0	47.0	60.0	67.0
Ag/Al–Gd-2	6.0	35.0	61.0	73.0	81.0
Ag/Al–Gd-5	3.0	40.0	67.0	78.0	87.0
Al–Gd-15	10.0	31.0	66.0	81.0	87.0
Ag/Al–Gd-15	2.0	49.0	80.0	89.0	93.0
Ag/Al–Gd-25	5.0	35.0	65.0	90.0	95.0
Ag/Al–Gd-50	3.0	17.0	46.0	76.0	97.0
Ag/Gd_2O_3	5.0	0.0	0.0	23.0	61.0

15.0 and 25.0 wt% of Gd_2O_3 (Fig. 11). Table 2 shows the 4-chlorophenol photoconversion percentage exhibited by the materials. Pure γ-Al_2O_3 as support prepared by the sol–gel method photoconverted about 51.0% of 4-ClPh after 4 h of UV light irradiation. However, the photoconversion of 4-ClPh was improved by addition Gd_2O_3 to γ-Al_2O_3 as seen in the Al–Gd-15

Table 3 Rate constant (k) and half life time ($t_{1/2}$) of Ag/Al–Gd-x photocatalysts

Photocatalyst	$k \times 10^{-3}$ (min^{-1})	$t_{1/2}$ (h)
Al_2O_3	3.4	3.36
Ag/Al_2O_3	9.1	1.27
Ag/Al–Gd-2	3.4	39
Ag/Al–Gd-5	9.3	24
Al–Gd-15	9.5	1.22
Ag/Al–Gd-15	13.8	84
Ag/Al–Gd-25	14.5	80
Ag/Al–Gd-50	8.0	44
Ag/Gd_2O_3	1.6	7.00

composite oxide, photoconverting about 87.0% after 4 h of reaction and by coupling silver onto Al–Gd-x composite oxide supports (Table 2). The photo-conversion percentage of 4ClPh increased with Gd_2O_3 concentration in the Ag/Al–Gd-x photocatalysts. Comparatively, the maximum photo-conversion of 4-ClPh (67.0%) obtained by Ag/Al after 4 h of UV light irradiation was reached in less time when Gd_2O_3 was added to alumina to obtain Ag/Al–Gd-x photocatalysts (Table 2). The maximum photoconversion of 4-ClPh (~90%) was observed in Ag/Al–Gd-15 and Ag/Al–Gd-25 photocatalysts after 3 h of UV light irradiation improving the photoconversion percentage in approximately 50.0% with respect to that of Ag/Al (Table 2). At higher Gd_2O_3 concentration the photoconversion of 4-ClPh decreased to 76.0% in Ag/Al–Gd-50 and 23.0% in the bare Ag/Gd_2O_3 photocatalyst after 3 h of UV light irradiation.

The kinetics data of 4-ClPh photo-degradation reaction at 3 h of UV light irradiation over Ag/Al–Gd-x photocatalysts were fitted to a pseudo first-order equation using the Langmuir–Hinshelwood model that has been often used to describe the kinetics of photocatalytic reactions of organic compounds in aqueous medium:[56,57]

$$\ln(C_0/C) = k_{app}t \quad (1)$$

The $\ln(C_0/C)$ *versus* reaction time (t) plots are linear (Fig. 12) indicating that photo-degradation kinetics adjusts well to a pseudo first-order equation. With the increase in Gd_2O_3 concentration in Ag/Al–Gd-x, the photocatalytic activity improved as shown by an increase in the reaction rate constant (k) and a decrease in the half-life time ($t_{1/2}$) (Table 3). The kinetic studies confirms that Ag/Al–Gd-x photocatalysts with concentrations of 15.0 and 25.0 wt% of Gd_2O_3 are the materials with the highest efficiency for the elimination of 4-ClPh in aqueous medium as corroborated by their higher reaction rate constants and their lower half-life times in the photocatalysts series (Table 3).

In order to figure out the efficacy of the materials to mineralize dissolved carbon to CO_2 during photodegradation of 4-ClPh, it was determined the total organic carbon (TOC) (Fig. 13). A continuous decrease in the relative concentration (C/C_0) of organic carbon with the UV light irradiation time was observed indicating the mineralization of dissolved organic carbon to CO_2. Ag/Al_2O_3 mineralized about 32.0% of dissolved carbon

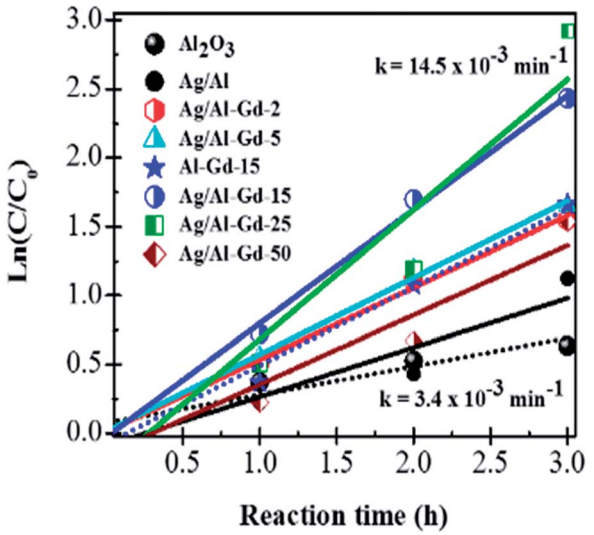

Fig. 12 $\ln(C_0/C)$ *vs.* reaction time in the photodegradation of 4-chlorophenol after 3 h of UV light irradiation using Ag/Al–Gd-x photocatalysts.

after 4 h of UV light irradiation. However, when Ag/Al–Gd-x were used as photocatalysts, the mineralization of dissolved carbon to CO_2 increased with Gd_2O_3 concentration and more than 78.0% of dissolved carbon was mineralized to CO_2 using Ag/Al–Gd-x photocatalysts with Gd_2O_3 concentration higher than 15.0 wt% after 4 h of UV light irradiation.

The identification of residual intermediaries was carried by calculation of the concentration of the possible intermediaries, 1,4-benzoquinone and hydroquinone, at the wavelengths of 245.0 and −283.0 nm respectively as we reported previously for phenol photodegradation using Al_2O_3–Nd_2O_3–ZnO composite oxides.[58] Fig. S4† shows the UV-Vis spectra of 4-ClPh degradation after 6 h of UV light irradiation using the Ag/Al–Gd-25 photocatalyst. This figure also depicts the possible

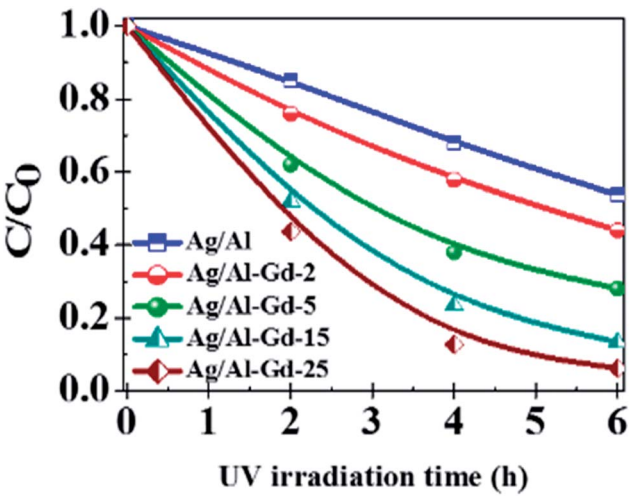

Fig. 13 Relative concentration of total organic carbon as a function of the UV light irradiation time of 4-chlorophenol solution over Ag/Al–Gd-x photocatalysts.

intermediaries 1,4-benzoquinone and hydroquinone at the wavelength of 245.0 and 283.0 nm respectively. Whereas, Fig. S5† shows the relative concentration (C/C_{max}) *vs.* reaction temperature for a period of 6 h of UV light irradiation. The calculated concentration values of 1,4-benzoquinone, hydroquinone and 4-chlorophenol as a function of the UV light irradiation time are shown in Table S1.† It can be observed that the relative concentration of 4-ClPh decreases nearly to cero after 4 h of UV light irradiation from 6.65×10^{-4} mol L^{-1}. Whereas, the hydroquinone formed is maximum at 1 h of UV light irradiation with a concentration of 1.61×10^{-4} mol L^{-1} and decreases to cero after 4 h of UV light irradiation. The formation of 1,4-benzoquinone was nearly negligible in the photodegradation of 4-ClPh decreasing from 1.20×10^{-5} mol L^{-1} to 2.57×10^{-6} mol L^{-1} after 4 h of UV light irradiation.

Influence of coupling Ag and Gd_2O_3 on the improvement in the photocatalytic activity of Ag/Al–Gd-*x* photocatalysts in the degradation of 4-ClPh

Silver was coupled onto Al_2O_3–Gd_2O_3 composite oxides prepared by the sol–gel method giving rise to a high dispersion of metallic silver particles and an intimate contact between species. Nano- and micro-particles of metallic silver or possibly silver quasi-crystals of irregular pentagonal shape intersected by plane nanobelts of Al_2O_3–Gd_2O_3 were observed by SEM of the Ag/Al–Gd-25 photocatalyst. Such chemical state might ease the electronic transfer from Al_2O_3–Gd_2O_3 composites to metallic silver due to the strong interaction between phases. Thus, the improvement in the photocatalytic activity of silver photocatalysts supported on Al_2O_3–Gd_2O_3 composite oxides might depends on the interaction extent between silver particles and Al_2O_3–Gd_2O_3 composite oxide as evidenced in the more active Ag/Al–Gd-25 photocatalyst. This is explained because the strong interaction between phases might ease the overlap of their electronic bands. In this sense, the improvement in the photocatalytic activity of Ag/Al–Gd-*x* photocatalysts would be proportional to the concentration of Gd_2O_3 in the Al_2O_3–Gd_2O_3 composite oxides that is interacting with silver nano- and micro-particles. It is presumable that when Ag/Al–Gd-*x* photocatalysts are irradiated with UV light, electrons (e^-) are excited from the valence band of γ-Al_2O_3 to the incomplete "4f" orbital of Gd_2O_3 and to the conduction band of metallic silver particles leaving a positively charged region (h^+) in the γ-Al_2O_3. This assumption is supported because a decrease in the band gap energy of γ-Al_2O_3 induces a decrease in the position of the Fermi level that can be correlated with an increase in ability of γ-Al_2O surface to give electrons.[59] In this work, the calculated band gap energy for γ-Al_2O_3 prepared by the sol–gel method has a value of 3.59 eV which is considerably lower than that reported for insulators materials which is typically above 5.0 eV.[60] The decrease in the band gap energy of γ-Al_2O_3 and thereby its increase in the donor behaviour can cause the modification in its surface chemistry.[59] In the γ-Al_2O_3 prepared by the sol–gel method there is a decrease in its band gap energy implying that there is an increase in the ability of its surface to give electrons (e^-) and leaving a high amount of holes (h^+) under UV light irradiation. Furthermore, it is known that in Gd_2O_3, the *f*-levels appear as resonances within the valence and conduction bands.[61] In rare earth oxides such as Gd_2O_3, the valence band refers to the occupied O p-states, while the conduction band is comprised of mainly "d" character.[62] Moreover, it is also proposed that in oxides like γ-Al_2O_3, the "sp" band of aluminum hybridizes with the "p" orbitals of oxygen giving rise to a hybridized new band.[63] The lower part of this new band is the valence band and the upper part is the conduction band, whereas the separation between them is the band gap of γ-Al_2O_3. Therefore, due to the overlap of electronic bands of different phases for high Gd_2O_3 concentration in the Ag/Al_2O_3–Gd_2O_3 photocatalysts, both Gd_2O_3 and metallic silver might act as traps of electrons (e^-) arriving from the valence band of γ-Al_2O_3 after excitation with UV light irradiation. Whereas, γ-Al_2O_3 phase might act as a trap of holes (h^+) after excitation with UV light irradiation. Thus, the role of Ag^0 and Gd_2O_3 phases in Ag/Al_2O_3–Gd_2O_3 photocatalysts would be to retard the electron–hole pair recombination rates. This assumption is corroborated by fluorescence spectroscopy of Ag/Al–Gd-*x* photocatalysts. Fig. 14 shows the emission spectra of Ag/Al, Ag/Al–Gd-*x* and Ag/Gd after excitation with a wavelength of 250.0 nm. Whereas, inset in Fig. 14 shows the emission spectra of Al_2O_3, Gd_2O_3 and Al–Gd-*x* composite oxides. With the exception of the emission spectra of Al–Gd-2, Ag/Al–Gd-2 and pure Gd_2O_3, the intensity of emission spectra of Al–Gd-*x* composite oxides and Ag/Al–Gd-*x* photocatalysts decreased significantly with respect to that of bare Al_2O_3, Gd_2O_3 and Ag/Al_2O_3 respectively implying that the recombination rate of electron–hole pairs is effectively decreased by adding Gd_2O_3 to Al_2O_3 and by depositing silver onto Al–Gd-*x* composite oxides to obtain Ag/Al–Gd-*x* photocatalysts. It is observed that Ag/Al–Gd-25 and Ag/Al–Gd-50 have the lower intensity of the emission spectra, being lower even than that of bare Ag/Gd_2O_3. This fact indicates that the recombination rate of photo-induced electron charge was highly inhibited in the Ag/Al–Gd-*x* photocatalysts with high concentration of Gd_2O_3 (x > 15 wt%) and confirms that the strong interaction between silver particles and Al_2O_3–Gd_2O_3

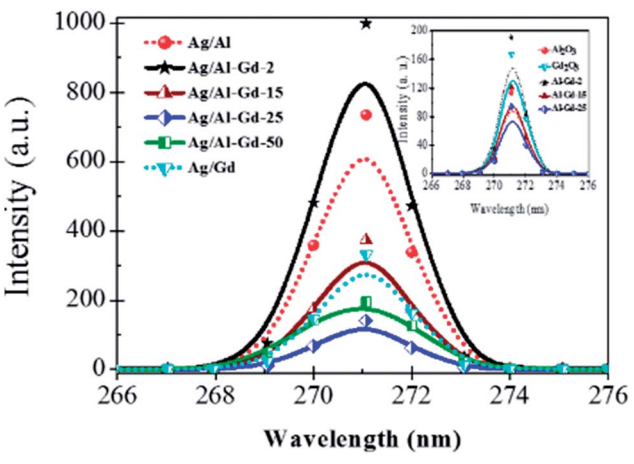

Fig. 14 Fluorescence spectra of Ag/Al–Gd-*x* photocatalysts prepared by the sol–gel method.

composite oxides favors the separation of photo-induced charge (e^- and h^+). The improvement in the photocatalytic activity of Ag/Al–Gd-*x* photocatalysts compared to those of bare Ag/Al_2O_3 or pure Al_2O_3 and Gd_2O_3 could be also explained if we consider these materials prepared by the sol–gel method as co-catalysts where there is a synergetic effect of spatial transfer of photo-generated charges as reported recently by some authors for silver co-catalysts.[64–66] In this sense, Al_2O_3 might work as a hole co-catalyst, whereas Ag and Gd_2O_3 might function as electron co-catalysts providing the reaction sites for the photo-degradation of 4-ClPh molecules. Other interesting property of Ag/Al–Gd-*x* photocatalysts with high concentration of Gd_2O_3 ($\geq$25.0 wt%) is that their UV-Vis spectra (Fig. 6) shows absorption bands attributed to surface plasmon resonance of metallic silver nanoparticles. In this sense, the separation of photo-induced charge (e^- and h^+) arisen from the interaction between metallic silver nanoparticles and Al_2O_3–Gd_2O_3 composite oxides could be linked to surface plasmon and charge transfer states of metallic silver particles as suggested also from the XPS spectrum of Ag/Al–Gd-25 photocatalyst (Fig. 7B). This observation also confirms that nano- and micro-particles of Ag^0 and Gd_2O_3 act as electron tramps favoring the decrease in the recombination rate of electron–hole pairs. In this sense, under UV light irradiation of Ag/Al–Gd-*x* photo-catalysts, photo-excited electrons (e^-) would be caught by metallic silver and Gd_2O_3, whereas holes (h^+) would be captured by γ-Al_2O_3 in a similar process as that reported for plasmonic photocatalysis.[67] As result of photo-induced charges separation, the photo-excited electrons and holes would migrate to the Ag/Al–Gd-*x* photocatalyst surface to initiate the photodegradation reaction of ClPh molecules. Furthermore, the amount of surface OH^- groups decreased with the increase in the concentration of Gd_2O_3 in the materials as inferred from the FTIR spectra of Ag/Al–Gd-*x* photocatalysts (Fig. 9). This fact suggests, that Ag/Al–Gd-*x* photocatalysts with high concentration of Gd_2O_3 might also contain a high density of surface anion vacancies and consequently a higher capability to adsorb OH^- groups during photoreaction, therefore increasing the photocatalytic activity of the materials in the photodegradation of 4-ClPh in aqueous medium.

Conclusions

The photocatalytic activity in the degradation of 4-chlorophenol with UV-ligh irradiation using 2.0 wt% Ag/Al_2O_3–Gd_2O_3 photo-catalysts prepared by the sol–gel method was studied. Bare Ag/γ-Al_2O_3 exhibited high photocatalytic activity, photoconverting about 67.0% of 4-chlorophenol after 4 h of UV light irradiation. However, the photocatalytic activity of Ag/Al_2O_3 was improved with addition of Gd_2O_3 to γ-Al_2O_3 by the sol–gel method to obtain Ag/Al_2O_3–Gd_2O_3 photocatalysts. Ag/Al–Gd-*x* with 15.0 and 25.0 wt% of Gd_2O_3 were the photocatalysts with the highest efficacy to photodegradate 4-chlorophenol photoconverting about 90.0% of 4-chlorophenol and mineralizing more than 85.0% of dissolved organic carbon after 4 h of UV light irradiation. Ag/Al_2O_3–Gd_2O_3 photocatalysts with high concentration of Gd_2O_3 ($\geq$15.0 wt%) favors the decrease in the recombination rate of photo-induced charges (e^- and h^+) due to that the strong interaction between silver nanoparticles and microparticles and Al_2O_3–Gd_2O_3 composite oxide supports induces the separation of charges. The role of silver and Gd_2O_3 in the Ag/Al_2O_3–Gd_2O_3 photocatalysts is to act as electron tramps favoring the decrease in the recombination rate of photo-induced electron–hole pairs.

Conflicts of interest

The authors declare no competing financial interest.

Acknowledgements

This work was partially supported by grants from COECYTJAL (Project: PS-09-2009-732), CONACYT (Project: 119058) and PROSNI. J. E. Casillas is indebted to CONACYT for granting a scholarship (CONACYT scholar No. 287873).

Notes and references

1 M. T. Pinho, H. T. Gomes, R. S. Ribeiro, J. L. Faria and A. M. Silva, *Appl. Catal., B*, 2015, **165**, 706–714.
2 E. Saputra, S. Muhammad, H. Sun, H. M. Ang, M. O. Tadé and S. Wang, *Appl. Catal., B*, 2013, **142–143**, 729–735.
3 L. Qi, H. You, Z. Zhang, S. Feng and S. S. van Agtmaal, *Int. J. Electrochem. Sci.*, 2013, **8**, 5457–5468.
4 M. F. Almeida, C. R. Bellato, A. H. Mounteer, S. O. Ferreira, J. L. Milagres and L. D. L. Miranda, *Appl. Surf. Sci.*, 2015, **357**, 1765–1775.
5 J. J. Murcia, M. C. Hidalgo, J. A. Navío, J. Araña and J. M. Doña-Rodríguez, *Appl. Catal., B*, 2015, **179**, 305–312.
6 S. H. Lin, C. H. Chiou, C. K. Chang and R. S. Juang, *J. Environ. Econ. Manag*, 2011, **92**, 3098–3104.
7 Y. Hu, D. Li, F. Sun, Y. Weng, S. You and Y. Shao, *J. Hazard. Mater.*, 2016, **301**, 362–370.
8 A. Mantilla, G. Jacome-Acatitla, G. Morales-Mendoza, F. Tzompantzi and R. Gomez, *Ind. Eng. Chem. Res.*, 2011, **50**, 2763–2768.
9 G. Mendoza-Damián, F. Tzompantzi, A. Mantilla, A. Barrera and L. Lartundo-Rojas, *J. Hazard. Mater.*, 2013, **263**, 67–72.
10 F. Tzompantzi, Y. Piña, A. Mantilla, O. Aguilar-Martinez, F. Galindo-Hernández, X. Bokhimi and A. Barrera, *Catal. Today*, 2014, **220–222**, 49–55.
11 A. Barrera, F. Tzompantzi, V. Lara and R. Gómez, *J. Photochem. Photobiol., A*, 2012, **227**, 45–50.
12 A. Barrera, F. Tzompantzi, J. M. Padilla, J. E. Casillas, G. Jácome-Acatitla, M. E. Cano and R. Gómez, *Appl. Catal., B*, 2014, **144**, 362–368.
13 P. D. Cozzoli, R. Comparelli, E. Fanizza, M. L. Curri, A. Agostiano and D. Laub, *J. Am. Chem. Soc.*, 2004, **126**, 3868–3879.
14 P. V. Kamat, M. Flumiani and A. Dawson, *Colloids Surf., A*, 2002, **202**, 269–279.
15 V. Subramanian, E. Wolf and P. V. Kamat, *Langmuir*, 2003, **19**, 469–474.
16 A. Dawson and P. V. Kamat, *J. Phys. Chem. B*, 2001, **105**(5), 960–966.

17 A. Wood, M. Giersig and P. Mulvaney, *J. Phys. Chem. B*, 2001, **105**, 8810–8815.
18 V. Subramanian, E. E. Wolf and P. V. Kamat, *J. Phys. Chem. B*, 2003, **107**(30), 7479–7485.
19 M. Jakob, H. Levanon and P. V. Kamat, *Nano Lett.*, 2003, **3**, 353–358.
20 H. Haick and Y. Paz, *J. Phys. Chem. B*, 2003, **107**, 2319–2326.
21 Z. Zhang, C. C. Wang, R. Zakaria and J. Y. Ying, *J. Phys. Chem. B*, 1998, **102**, 10871.
22 H. Kominami, S. Muratami, J. Kato, Y. Kera and B. Ohtani, *J. Phys. Chem. B*, 2002, **106**(40), 10501–10507.
23 A. Roucoux, J. Schlz and H. Patin, *Chem. Rev.*, 2002, **102**, 3757–3778.
24 A. Szucs, F. Berger and I. Dekany, *Colloids Surf., A*, 2000, **174**, 387–402.
25 S. K. Ghosh, S. Kundu, M. Mandal and T. Pal, *Langmuir*, 2002, **18**(23), 8756–8760.
26 L. Gang, B. G. Anderson, J. Grondelle, J. van Grondelle and R. A. van Santen, *Appl. Catal., B*, 2002, **40**, 101–110.
27 R. M. Dickson and L. A. Lyon, *J. Phys. Chem. B*, 2000, **104**(26), 6095–6098.
28 Y. Sun and Y. Xia, *Science*, 2002, **298**, 2176–2179.
29 R. C. Jin, Y. W. Cao, C. A. Mirkin, K. L. Kelly, G. C. Schatz and J. G. Zheng, *Science*, 2001, **294**, 1901–1903.
30 R. Jin, Y. C. Cao, E. Hao, G. Metraux, G. C. Schatz and C. A. Mirkin, *Nature*, 2003, **425**, 487–490.
31 M. I. Ghouri, E. Ahmed, N. R. Khalid, M. Ahmad, M. Ramzan, A. Shakoor and N. A. Niaz, *J. Ovonic Res.*, 2014, **10**(3), 89–100.
32 Y. B. Losovyj, D. Wooten, J. C. Santana, J. M. An, K. D. Belashchenko, N. Lozova, J. Petrosky, A. Sokolov, J. Tang, W. Wang, N. Arulsamy and P. A. Dowben, *J. Phys.: Condens. Matter*, 2009, **21**, 045602.
33 H. Guo, X. Yang, T. Xiao, W. Zhang, L. Lou and J. Mugnier, *Appl. Surf. Sci.*, 2004, **230**, 215–221.
34 S. Lowell, J. E. Shields and M. A. Thomas, in, *Characterization of Porous Solids and Powders: Surface Area, Pore Size and Density*, ed. M. Thommes, Springer, Netherlands, 2004, pp. 31–32.
35 K. W. S. Sing, D. H. Everet, R. A. W. Haul, L. Moscou, R. A. Pierotti, J. Rouquerol and T. Siemieniewska, *Pure Appl. Chem.*, 1985, **57**, 603–619.
36 G. Pérez, S. Fuentes, V. Petranovskii and A. Simakov, *Catal. Lett.*, 2006, **110**, 53–60.
37 S. Hazarika, N. Paul and D. Mohanta, *Bull. Mater. Sci.*, 2014, **37**(4), 789–796.
38 C. Hu, T. Peng, X. Hu, Y. Nie, X. Zhou, J. Qu and H. He, *J. Am. Chem. Soc.*, 2010, **132**(2), 857–862.
39 N. Bogdanchikova, F. C. Meunier, M. Avalos-Borja, J. P. Breen and A. Pestryakov, *Appl. Catal., B*, 2002, **36**, 287–297.
40 Z. Li and M. F. Stephanopoulos, *J. Catal.*, 1999, **182**(2), 313–327.
41 C. Hu, T. Peng, X. Hu, Y. Nie, X. Zhou, J. Qu and H. He, *J. Am. Chem. Soc.*, 2010, **132**, 857–862.
42 A. Barrie and N. E. Christensen, *Phys. Rev. B: Condens. Matter Mater. Phys.*, 1976, **14**(6), 2442–2447.
43 N. Bowering, D. Croston, P. G. Harrisson and G. S. Walker, *Int. J. Photoenergy*, 2007, 1–8.
44 B. V. Crist, *Handbook of Monochromatic XPS Spectra, Commercially Pure Binary Oxides*, XPS International Inc., 1999, vol. 2, pp. 37–42.
45 C. D. Wagner, W. M. Riggs, L. E. Davis, J. F. Moulder and G. E. Muilendberg, *Handbook of X-ray photoelectron spectroscopy*, Perkin Elmer, Eden Prairie, 1992.
46 A. T. M. A. Rahman, K. Vasilev and P. Majewski, *J. Colloid Interface Sci.*, 2011, **354**, 592–596.
47 D. D. Sarma and C. N. R. Rao, *J. Electron Spectrosc. Relat. Phenom.*, 1980, **20**, 25–45.
48 B. Zhang, H. Jin, Y. Li, B. Chen, S. Liu and D. Shi, *J. Mater. Chem.*, 2012, **22**, 14494–14501.
49 C. Solis, J. Rivera, C. J. Lucio-Ortiz, A. Hernández-Ramírez, F. Castillón and J. Sánchez-Valente, *Materials*, 2014, **7**, 2062–2086.
50 J. Kloprogge, L. V. Theo, L. V. Duong, B. J. Wood and R. L. Frost, *J. Colloid Interface Sci.*, 2006, **296**(2), 572–576.
51 P. Dufresne, E. Payen, J. Grimblot and J. P. Bonnelle, *J. Phys. Chem.*, 1981, **85**, 2344–2351.
52 T. L. Barr, *J. Phys. Chem.*, 1978, **82**(16), 1801–1810.
53 B. Strohmeier, *Surf. Sci. Spectra*, 1995, **3**(2), 135–140.
54 A. Nylund and I. Olefjord, *Surf. Sci. Spectra*, 1994, **22**, 283–289.
55 J. R. Lindsay, H. J. Rose, W. E. Swartz, P. H. Watts and K. A. Rayburn, *Appl. Spectrosc.*, 1973, **27**, 1–4.
56 A. Sobczynski, Ł. Duczmal and W. Zmudzinski, *J. Mol. Catal. A: Chem.*, 2004, **213**, 225–230.
57 K. Porkodi and K. V. Kumar, *Appl. Catal., B*, 2008, **79**, 108–109.
58 J. E. Casillas, F. Tzompantzi, S. G. Castellanos, G. Mendoza-Damián, R. Pérez-Hernández, A. López-Gaona and A. Barrera, *Appl. Catal., B*, 2017, **208**, 161–170.
59 B. Ealet, M. H. Elyakhloufi, E. Gillet and M. Ricci, *Thin Solid Films*, 1994, **250**, 92–100.
60 B. Shin, J. R. Weber, R. D. Long, P. K. Hurley, C. G. Van de Walle and P. C. MacIntyre, *Appl. Phys. Lett.*, 2010, **96**(15), 152908.
61 G. Scarel, A. Svane and M. Fanciulli, Scientific and Technological Issues Related to Rare Earth Oxides, *Rare Earth Oxide Thin Films: Growth, Characterization, and Applications*, ed. G. Scarel and M. Fanciulli. Topics in Appl. Phys., vol. 106, Springer-Verlag GmbH, Heidelberg, Germany, 2007.
62 H. B. Lal and K. Gaur, *J. Mater. Sci.*, 1988, **23**(3), 919–923.
63 M. Kefi, P. Jonnard, F. Vergand, C. Bonnelle and E. Gillet, *J. Phys.: Condens. Matter*, 1993, **5**(45), 8629–8642.
64 X. Wang, T. Li, R. Yu, H. Yu and J. Yu, *J. Mater. Chem. A*, 2016, **4**, 8682–8689.
65 H. Yu, R. Liu, X. Wang, P. Wang and J. Yu, *Appl. Catal., B*, 2012, **111**, 326–333.
66 R. Liu, P. Wang, X. Wang, H. Yu and J. Yu, *J. Phys. Chem. C*, 2012, **116**, 17721–17728.
67 X. Zhang, Y. L. Chen, R. S. Liu and D. P. Tsai, *Rep. Prog. Phys.*, 2013, **76**, 046401–046441.